KATARZYNA KOZIEŁ [ID][1*], JAKUB JANUS [ID][1]

FORCE EXERTED BY GAS ON MATERIAL EJECTED DURING GAS-GEODYNAMIC PHENOMENA. ANALYSIS AND EXPERIMENTAL VERIFICATION OF THEORY

The analysis of natural hazards, including gas-geodynamic phenomena, requires study of the basic physical processes that take place at each stage of an event. This paper focuses on analysing the transport of fragmented rock material during rock and gas outbursts. Our theoretical considerations and experiments have allowed us to specify and verify the significant forces acting on fragmented rock during its transport, thus determining the speed of grains of each grain class in the stream of expanding gas. The above study may serve as a preface to a wide-ranging quantitative and qualitative energy analysis of the movement of material ejected during Gas-geodynamic phenomena.

Keywords: gas velocity; Force; rock and gas outburst; gas-geodynamic phenomena; ejected material

1. Introduction

The issue of rock and gas outbursts has been a problem in mining for over 150 years [1-5]. Rock and gas outbursts in mining involve the fragmentation of originally solid rock and the dynamic displacement of fragmented material along mine headings. The main source of energy that causes the destruction and transportation of rock is gas filling the pores and fractures inside the rock [5-7]. Coal outbursts have been studied for many years, whereas virtually no research has been done on similar phenomena in other types of rock, in particular dolomite. Authors of many studies on coal and gas outburst assume that desorbed gas plays a key role in the process of transporting post-outburst coal masses [8-10]. Systematically increasing surface area of crushed coal causes intensification of desorption and release of new amounts of gas, which fluidly transports the masses deep into the excavation [11]. In rocks such as dolomite, soprtion is negligible and the

multitude of physical phenomena involved in an outburst and the degree of their complexity and interdependence are enormous. The only consideration of the transport of post-outburst masses of rocks such as dolomite is found in the work by Topolnicki and Wierzbicki [12]. The authors assume that the transport of rock masses is sedimentary in nature. They start their considerations with the condition of activation of a grain resting on crushed rock. They also determine the theoretical thrust force of a gas stream, which would allow launching a hay with a given surface area. There is a great convergence of approaches to post-outburst mass transport, but Topolnicki and Wierzbicki [12] presented only theoretical considerations, not supported by experimental studies.

The assumption made by the present authors is that the process of rock and gas outburst involves the release of energy during the rapid decompression of gas in pores and crevices inside the rock. The thermodynamic transformation that takes place during decompression is close in nature to an isothermal process [13,14]. Such enormous energy leads to the fragmentation of solid rock [13]. Fragmented rock material falls to the lowermost part of the mine heading due to the effect of gravity, simultaneously creating a post-outburst cavern in the roof of the heading. The gas released from the cavern flows above the deposited rock pile. As the opening of the heading becomes choked with rock material, space for the gas to flow becomes constricted, resulting in an increase in the speed of the gas. The gas stream presses against the external layer of deposited grains of the rock material. When the speed of the gas, and consequently the force exerted by the gas stream, increases to the point where it exceeds the value of the forces keeping the rock grains immobile, the transport of rock material down the mine heading begins.

This paper focuses on analysis of the initiation of transport of fragmented rock. All forces acting on a single grain positioned on the deposited material have been analysed.

2. Gas-geodynamic phenomena

The first dolomite and gas outburst took place in the KGHM Rudna copper ore mine in Poland in 2009 [13]. As a result of the incident, ejected rock material was transported approximately 60 metres down the mine heading. Another incident on a similarly large scale was recorded in 2018, also in the Zagłębie Miedziowe region. This incident resulted in ejected rock material being deposited along approximately 30 metres of the mine heading. As of today, several hundred less severe Gas-geodynamic phenomena have been recorded in copper mines in the Legnica-Głogów Copper Belt (LGOM), including cave ceiling collapses and sudden outflows of gas from boreholes [15].

Apart from Gas-geodynamic phenomena in dolomite, where the ejection of fragmented rock is not caused by absorbed gas, outbursts have also been recorded in salt and potassium mines [16-18]. Rock and gas outbursts in salt and potassium mines are a worldwide phenomenon. Material ejected during an outburst at the Menzengraben mine in Germany in 1953 included over 4500 m^3 of cracked rock salt. There have been over 200 outbursts recorded in Russian salt and potassium mines, with the mass of ejected material reaching up to approximately 4500 tonnes [19]. Rock and gas outbursts have also been recorded in potassium salt deposits in Romania [20]. The most recent rock and gas outburst was recorded at the Boulby potassium salt mine in England in 2016, resulting in the death of one employee. In Polish salt mines, the danger posed by rock and gas outbursts has been documented in the Kłodawa mine [21].

Outbursts from sandstone forms located under coal deposits are relatively frequent [22]. Sandstone-gas outbursts are some of the most dangerous hazards encountered in underground engineering [23]. A sandstone and gas outburst that took place at the Haishiwan mine in China

released over 900,000 m³ of gas, with 2000 tonnes of sandstone being ejected as a result. Another example is the Phalen mine in Canada, where a total of five sandstone and gas outbursts took place between 1994 and 2000 [23]. Sandstone and gas or salt and gas outbursts have also been recorded in copper ore mines [24]. The essential differences between coal and sandstone, dolomite or anhydrite, which may affect the initiation of Gas-geodynamic phenomena, result primarily from the sorption properties, chemical composition and mechanical parameters of these rocks [25-30].

3. Theory behind the transport of ejected material

The transport of ejected material is caused by adsorbed gas or free gas found in the pores and crevices of fragmented rock. Adsorbed gas plays a key role in the transport of fragmented coal. After coal is fragmented into very small grains, a forceful desorption of sorptively bound gas takes place. This creates the conditions necessary for fluidized transport to commence. Due to the negligible sorption in the case of dolomite and the much larger grain size, it is necessary to make a separate analysis of the triggering of the transport of rock material based on advection.

Based on an analysis of the profile of ejected material, we assume that its transport involves several stages:

I) as a result of sudden decompression, the gas found in the pores and crevices in the rock is released from the rock, destroying it simultaneously,

II) fragmented rock material falls to the lowermost part of the mine heading due to the effect of gravity, gradually choking the opening of the mine heading,

III) a stream of gas flows over the external layer of the deposited rock pile, pressing against the grains situated on the surface of the pile,

IV) if the gas flow rate reaches a critical value, which depends on the area of the cross-section of the mine heading that remains unobstructed by the rock pile and the stream of gas released from the fragmented rock mass, transport of the grains will be triggered.

3.1. Theoretical analysis of the force exerted by the gas stream

Certain assumptions need to be made when analysing the initiation of transport of a single grain. A stream of gas presses against the analysed single grain located on the surface of the deposited rock pile. For the grain to be transported further down the mine heading, the force of the gas stream must be greater than the forces acting on the grain and anchoring it to the deposit. These forces include gravity and reactions with neighbouring grains. The surface of the grain is subjected to a force exerted by the gas stream, resulting from the flow rate of the gas, its density, and the surface area on which it acts. The force can be expressed using the following formula (1):

$$F_N = S \cdot \frac{\rho v^2}{2} \tag{1}$$

where:

F_N — the force exerted by the gas stream on the grain, [N];

S — the average cross-sectional area of the grain on which the gas stream acts, [m²];

ρ — the gas density, [kg/m³];

v — the gas stream flow rate, [m/s].

494

However, assuming that the grain in question is not on a flat surface but lies between other adjoining grains of different sizes, an adjustment for the surface area of the grain directly subjected to the action of the gas stream must be made when determining the actual force exerted on the grain. For this purpose, a grain 'exposure coefficient', k, has been introduced, which reduces the grain's surface area to the actual surface subjected to the action of the gas stream. After accounting for the k coefficient, formula (1) now takes the form as specified in (2):

$$F_N = k \cdot S \cdot \frac{\rho v^2}{2} \tag{2}$$

where: k is the grain exposure coefficient, [–].

The front area of the grain subjected to pressure exerted by the gas was determined separately for each grain class, as the average value obtained when measuring the surface areas of 10 grains. Surface areas of grains were measured using a laser height gauge [31], the spatial orientation of each grain being randomly selected. Fig. 1 shows examples of cross-sections of grains from each grain class.
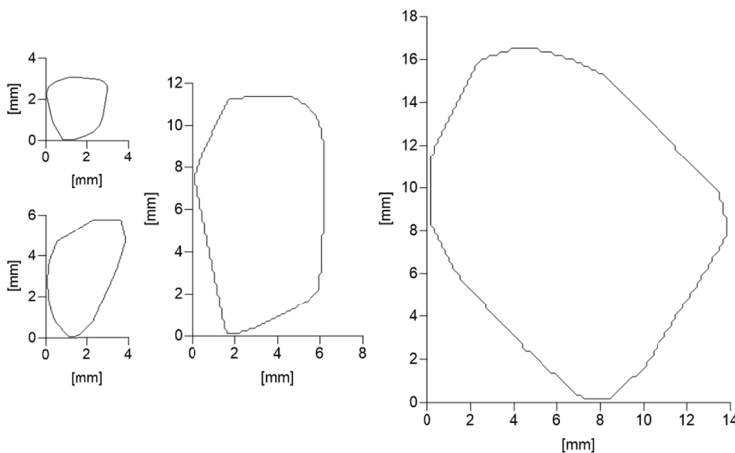

Fig. 1. Examples of cross-sections of grains from each grain class subjected to pressure

After being scanned, surfaces of grains from each grain class were measured using Surfer 11 software. Table 1 shows the results of measurement of cross-sections of grains from each grain class.

Based on our tests and their results, the force exerted by the gas stream on the front surface of the grain was determined for each of the four grain classes.

3.2. Experiment in a wind tunnel

The theoretical considerations concerning the force exerted on the front surface of the grain by the gas stream were verified in a wind tunnel [32].

Front surfaces of grains

Grain class [mm]	Grain surface area S [mm^2]	Grain class [mm]	Grain surface area S [mm^2]
1.0-2.0	8.27	2.0-4.0	16.21
	9.40		22.17
	8.36		29.21
	13.69		19.42
	11.90		26.04
	8.61		15.78
	9.96		17.00
	8.30		20.33
	9.74		17.58
	10.51		21.73
mean:	9.87	mean:	20.55
4.0-8.0	53.61	8.0-20.0	153.76
	34.22		118.83
	93.14		149.05
	68.13		129.37
	54.92		137.18
	81.71		83.62
	49.35		104.41
	101.72		115.64
	59.18		103.89
	72.20		140.82
mean:	66.82	mean:	123.66

The experiment was carried out using the wind tunnel at the Calibration Laboratory for Ventilation Measuring Instruments at the Strata Mechanics Research Institute of the Polish Academy of Sciences (Figs. 2-4), holding accreditation no. AP118 of the Polish Accreditation Centre [33,34]. An important feature of the wind tunnel is that it enables a stable flow of air in the measurement chamber within the 0.15 to 40 m/s range. Primary instruments used to measure flow rate include an orifice plate, used in the range of low velocities from 0.15 to 1.5 m/s, and a pitot-static tube, used in the range 1.5 to 40 m/s [35].

The air flow rate in the measurement chamber of the tunnel was measured by an indirect method using the pitot-static tube. A Betz projection manometer with a measurement range of 0-39.3 mbar and an accuracy of 0.01 mbar, holding a calibration certificate issued by an accredited laboratory, was used to measure the differential pressure on the tube. A μBAR electronic barometer and an Assman psychrometer were used to determine the current air density. The room was air-conditioned during the measurements, ensuring a stable ambient temperature.

The measurement kit was placed in the chamber, in a specially adapted grip that caused only small alterations to the air stream. By setting the fan rotation speed and measuring the differential pressure on the pitot tube, the appropriate air flow rate was then set.

The tested grains, representing four grain classes, were mounted on the ends of thin wires with diameter 0.3 mm and length 120 mm. The pendulums prepared in this way were placed inside
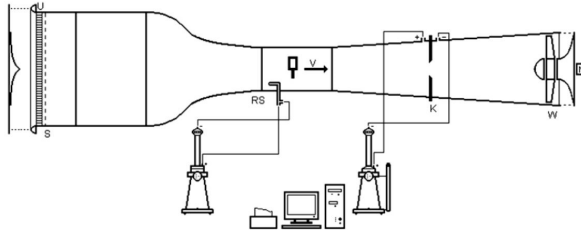
Fig. 2. Diagram of the wind tunnel at the Calibration Laboratory for Ventilation Measuring Instruments
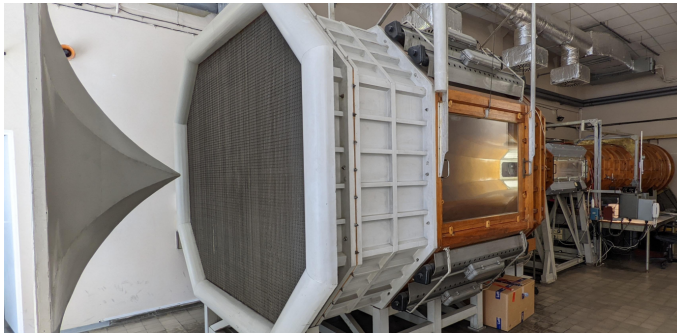U – honeycomb, S – mesh, RS – pitot tube, K – orifice plate, W – fan, N – fan motor

Fig. 3. Wind tunnel at the Calibration Laboratory for Ventilation Measuring Instruments

Fig. 4. Wind tunnel at the Calibration Laboratory for Ventilation Measuring Instruments

the wind tunnel. The angles of deflection of the pendulums depending on the set flow rate of the gas stream were the direct result of the experiments. This enabled the determination of the force exerted by the gas on the tested grains. The experiment offers great comparative opportunities with numerical methods using CFD methods [36,37].

Ten grains were randomly selected from each grain class. Tests of each grain class in the wind tunnel were repeated for three values of the gas stream flow rate. For the 1-2 mm grain class, the speeds were 3 m/s, 6 m/s and 9 m/s, for the 2-4 mm grain class the speeds were 5 m/s, 8 m/s

and 12 m/s, for the 4-8 mm grain class the speeds were 8 m/s, 12 m/s and 15 m/s, and for the largest (8-20 mm) grain class the speeds were 8 m/s, 15 m/s and 20 m/s. Fig. 5 shows a diagram of the measurement stand and photographs of the deflection of the wires during the experiment (Fig. 6). The force exerted by the gas on the front surface of the grain causes it to deflect; it is expressed using formula (3) and compared with the estimated gas force based on formula (2) for $k = 1$, where the value from Table 1 is used as the surface area of the cross-section of the grain S. The considerations disregarded the interaction of the air stream with the wire:

$$F_n = m_z \cdot g \cdot \tan \alpha \qquad (1)$$

where:

    F_n — the force exerted by the gas stream flowing around the grain, measured during the experiment, [N];

    m_z — the grain mass, [kg];

    α — the angle of deflection of the wire caused by the gas, [°].

Deflections of the grains were recorded using a video camera during the tests in the wind tunnel. The angle of deflection between the wire with the grain attached and the vertical plane were then determined using AutoCAD, and each angle was assigned to the relevant rock grain. The results of measured parameters (grain mass and recorded angles of deflection) are shown below (in Tables 2-5 and Figs 7-10) for each grain class.
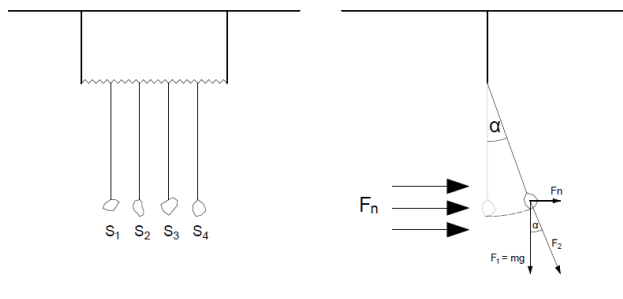

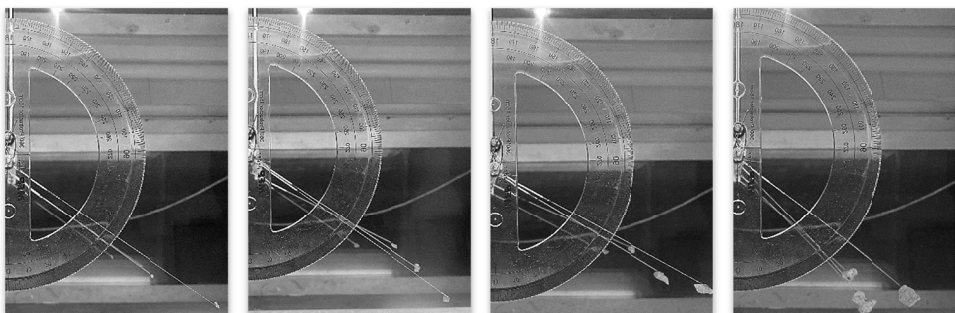Fig. 5. Diagram of the measurement stand in the wind tunnel (front and side views)

Fig. 6. Grains of various classes during the experiment in the wind tunnel

TABLE 2

Angles of deflection of a wire with a grain from the 1-2 mm grain class attached,
caused by the force in a wind tunnel

Flow rate		3 m/s	6 m/s	9 m/s
	Grain mass [g]	Angle of deflection of the wire with grain attached [°]		
1	0.02	16	47	65
2	0.01	14	47	68
3	0.02	13	46	63
4	0.02	15	47	64
5	0.03	14	45	66
6	0.02	18	49	70
7	0.01	14	47	67
8	0.02	13	46	64
9	0.03	15	46	65
10	0.02	11	47	63

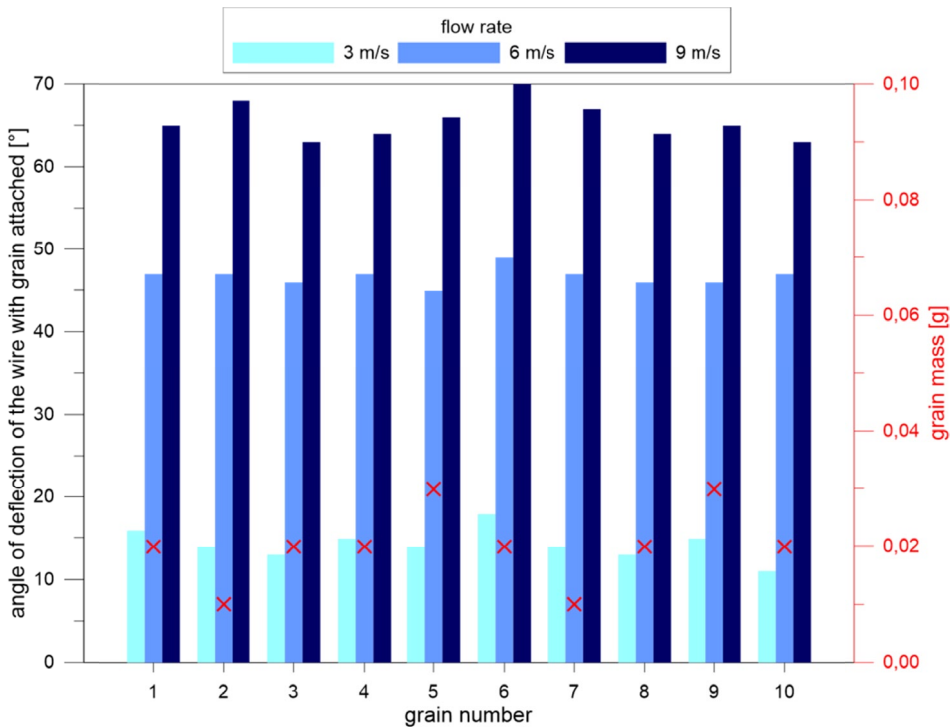
Fig. 7. Angles of deflection of a wire with a grain from the 1-2 mm grain class attached,
caused by the force in a wind tunnel

Angles of deflection of a wire with a grain from the 2-4 mm grain class attached,
caused by the force in a wind tunnel

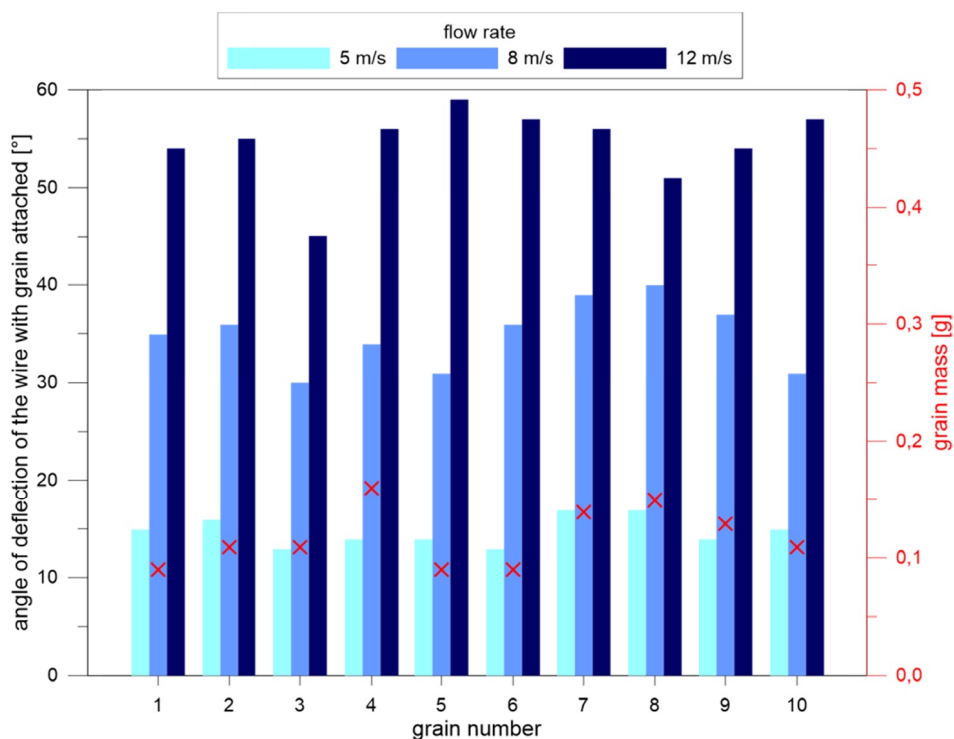| Flow rate		5 m/s	8 m/s	12 m/s
	Grain mass [g]	Angle of deflection of the wire with grain attached [°]		
1	0.09	15	35	54
2	0.11	16	36	55
3	0.11	13	30	45
4	0.16	14	34	56
5	0.09	14	31	59
6	0.09	13	36	57
7	0.14	17	39	56
8	0.15	17	40	51
9	0.13	14	37	54
10	0.11	15	31	57

Fig. 8. Angles of deflection of a wire with a grain from the 2-4 mm grain class attached,
caused by the force in a wind tunnel

TABLE 4

Angles of deflection of a wire with a grain from the 4-8 mm grain class attached,
caused by the force in a wind tunnel

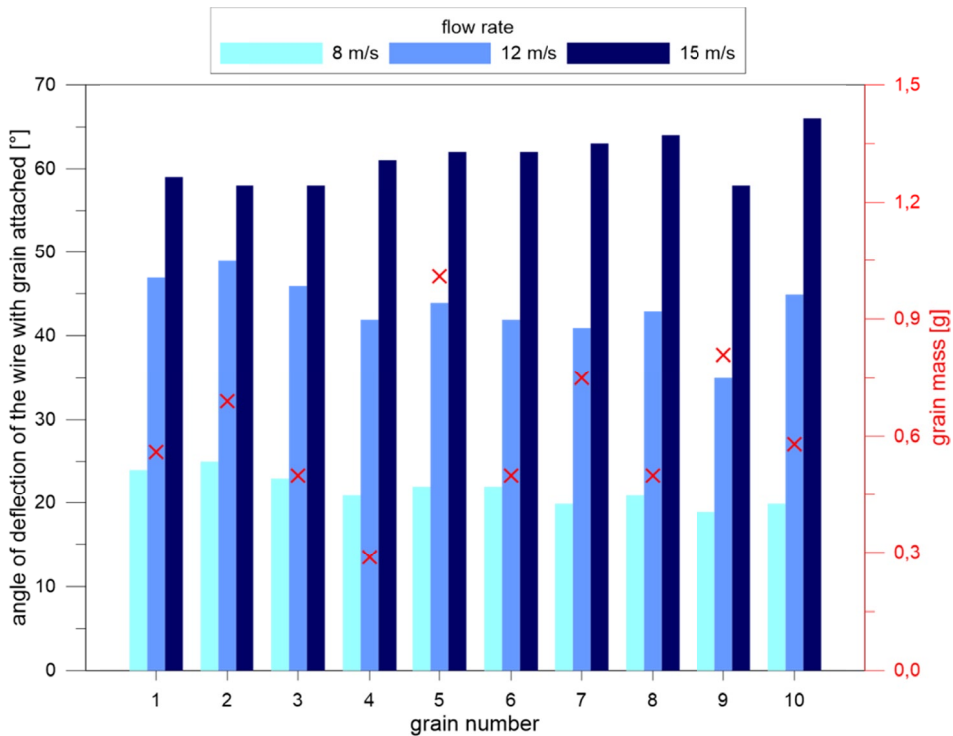| Flow rate		8 m/s	12 m/s	15 m/s
	Grain mass [g]	Angle of deflection of the wire with grain attached [°]		
1	0.56	24	47	59
2	0.69	25	49	58
3	0.50	23	46	58
4	0.29	21	42	61
5	1.01	22	44	62
6	0.50	22	42	62
7	0.75	20	41	63
8	0.50	21	43	64
9	0.81	19	35	58
10	0.58	20	45	66

Fig. 9. Angles of deflection of a wire with a grain from the 4-8 mm grain class attached,
caused by the force in a wind tunnel

TABLE 5

Angles of deflection of a wire with a grain from the 8-20 mm grain class attached,
caused by the force in a wind tunnel

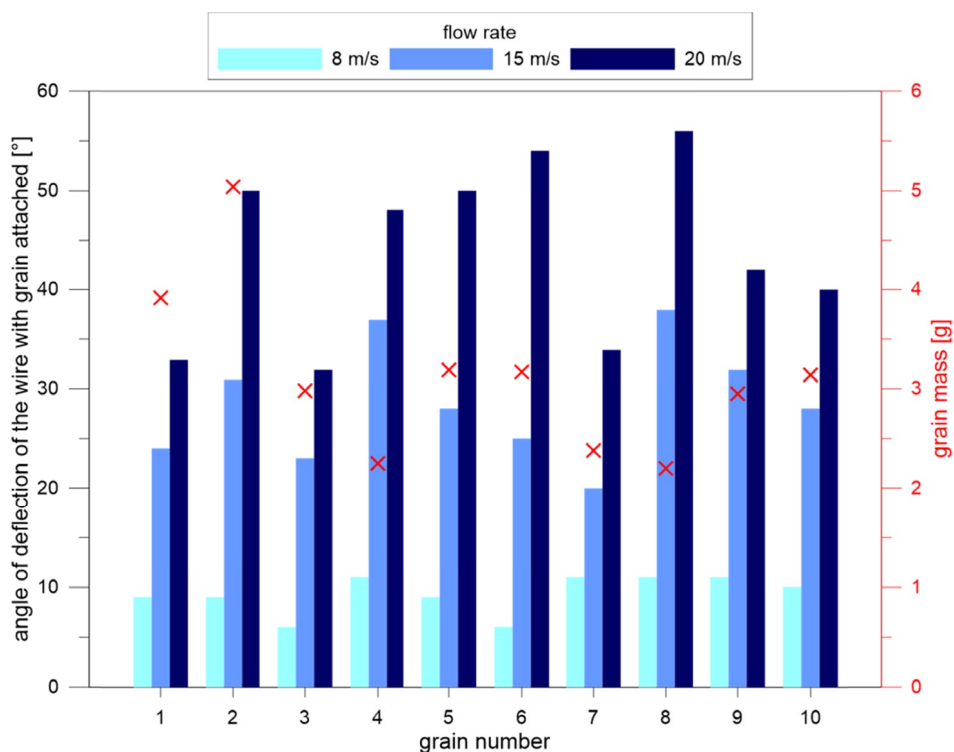| Flow rate		8 m/s	15 m/s	20 m/s
	Grain mass [g]	Angle of deflection of the wire with grain attached [°]		
1	3.92	9	24	33
2	5.04	9	31	50
3	2.98	6	23	32
4	2.25	11	37	48
5	3.20	9	28	50
6	3.18	6	25	54
7	2.38	11	20	34
8	2.20	11	38	56
9	2.95	11	32	42
10	3.15	10	28	40

Fig. 10. Angles of deflection of a wire with a grain from the 8-20 mm grain class attached,
caused by the force in a wind tunnel

502

These tests will enable determination of the force exerted by the gas stream on a grain placed inside a wind tunnel, depending on the size of the grain. Considerations concerning consistency between theory and experimental results are discussed in the next chapter.

3.3. Experimental verification of theory

Based on the measurements performed and results obtained, the force resulting from the deflection angle of a grain hanging on a wire was compared with the theoretical force dependent on the surface area of a grain subjected to a stream of gas. The estimated gas force was verified against the force obtained during the experiment in the wind tunnel using a percentage difference index. The percentage difference between the results was calculated as the difference of the experimentally determined force resulting from the deflection of the wire and the theoretical force, divided by the experimentally determined force; formula (4):

$$R = \frac{F_n - F_N}{F_n} \cdot 100 \tag{4}$$

where: R is the percentage difference index, [%].

Table 6 shows the force values determined experimentally and theoretically.

TABLE 6

Comparison of mean results of measurements of forces in the wind tunnel
and estimated force values

Grain class [mm]	Flow rate [m/s]	Force measured in the experiment [mN]	Theoretical gas force [mN]	Percentage difference [%]
	3	0.050	0.053	−6.2
1-2	6	0.208	0.213	−2.3
	9	0.431	0.480	−10.2
	5	0.311	0.308	0.9
2-4	8	0.821	0.789	4.1
	12	1.644	1.776	−7.4
	8	2.420	2.566	−5.7
4-8	12	5.752	5.773	−0.4
	15	11.070	9.021	22.7
	8	5.072	4.749	6.8
8-20	15	16.738	16.694	0.3
	20	29.530	29.678	−0.5

The experimentally and theoretically determined values of the forces are similar. In two cases, the percentage difference exceeds 10%. The variation in the percentage difference from −10.2% to 22.7% is primarily a result of the method used to attach the grain to the wire, and is also related to the centre of gravity of the attached grain and its spatial orientation. The mean percentage difference between the theoretical and experimental forces is approximately 0.2%.

The results obtained in the experiment indicate that the proposed theoretical force exerted by the gas stream on the grain enables the correct estimation of the force exerted by the gas stream on fragmented rock material during a rock and gas outburst.

3.4. Analysis of the speed of transport of grains in a gas stream

During transport, grains move along the mine heading. The motion of each grain is complex in nature. The grains collide with each other and with the walls of the mine heading. They settle on the surface of the deposit and are then again caught in the gas stream and carried deeper down the mine heading. According to the law of conservation of energy, after striking fragmented rock, the gas stream transfers some of its energy to the grains. The difference between the mean velocity of the grains and the flow rate of the gas stream depends on the size of the grains, and hence the force acting on them, and on the dynamic friction force:

$$F_N' > F_T \tag{5}$$

where:

F_N' — the force exerted on the grain in the air stream, [N];
F_T — the dynamic friction force, [N];

$$\frac{d_z^2 \cdot \rho \cdot (\Delta v)^2}{2} > g \cdot f_d \cdot d_z^3 \cdot \rho_s \tag{6}$$

$$\Delta v = \sqrt{2 \cdot g \cdot f_d \cdot d_z \cdot \frac{\rho_s}{\rho}} \tag{7}$$

where:

Δv — the difference between the grain transport velocity and the gas stream flow rate, [m/s];
g — gravitational acceleration, [m/s^2];
f_d — the dynamic friction coefficient [13], [–];
d_z — the equivalent grain diameter, [m];
ρ — the gas density, [kg/m^3];
ρ_s — the rock density, [kg/m^3].

The velocity of grain transport may be expressed using the following formula:

$$v_t = v_g - \sqrt{2 \cdot g \cdot f_d \cdot d_z \cdot \frac{\rho_s}{\rho}} \tag{8}$$

where:

v_t — the grain transport velocity, [m/s];
v_g — the measured mean gas stream flow rate, [m/s].

The test stand shown in Fig. 11 was constructed to analyse the transport of fragmented rock. The test involved the dynamic introduction of rock material into a gas stream. The experiment comprised multiple stages. Rock material of known mass was placed in a closed box constructed
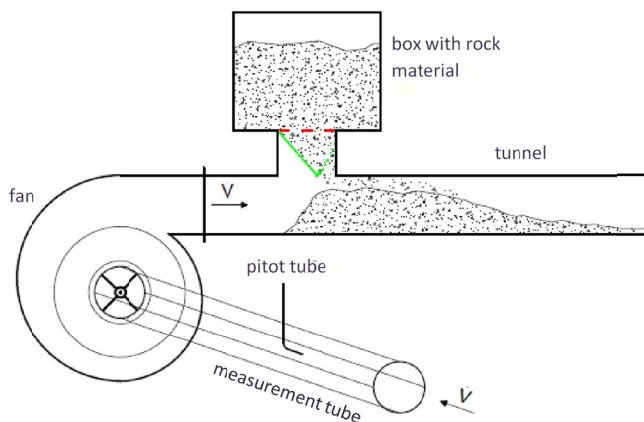
Fig. 11. Experiment to estimate the transport velocity of grains in the gas stream

above the tunnel. The fan was activated, and the box containing the material was then opened. The material fell to the bottom of the tunnel as a result of gravity, and was simultaneously lifted by the stream of flowing air and moved deeper down the tunnel. Due to the expansive nature of the dynamic experiment, the location where the velocity was measured was moved outside the tunnel. For this purpose, a three-metre PVC tube was attached at the fan inlet, where the air was sucked in. A pitot tube was placed axially at the midpoint of the tube. The purpose of inserting the tube was to provide separation from the turbulences caused by the fan and to enable measurement of the flow rate of the air blown into the tunnel.
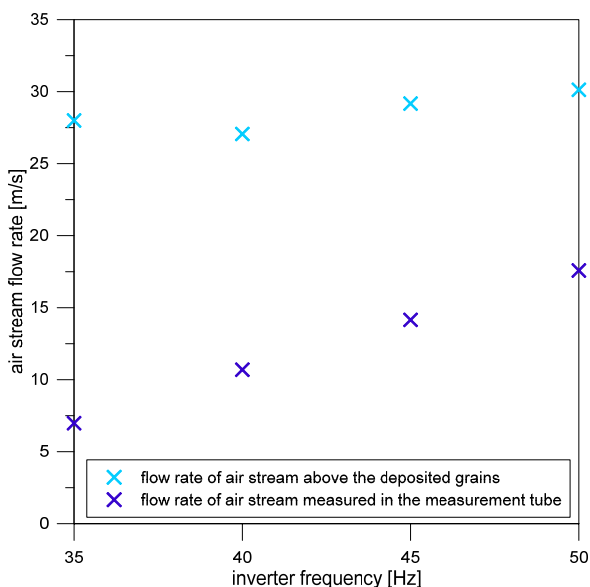

Fig. 12. Relation of flow rate measured in the measurement tube to the flow rate above the deposited grain pile

Experiments were performed for various flow rates of the air stream, regulated by adjusting the inverter frequency. Fig. 12 shows a graph of the measured averaged velocity in the measurement tube and the determined flow rate above the deposited grain pile against the fan speed, adjusted by means of the frequency of the inverter.

Irrespective of the set flow rate of the air stream pumped by the fan, the flow rate above the deposited grain pile is similar, which is a result of the fact that the transport of grains is triggered at the same flow rate in all experiments. The flow rate of the gas stream above the deposited pile was taken as the mean speed of measurements taken for various set frequencies of the inverter, hence a flow rate of $v_g = 28{,}6$ m/s.

When analysing the transport of a single grain, numerical values corresponding to the measurements obtained were substituted into equation (8). Equation (9) is a sample calculation for the grain size most commonly found in material ejected during outbursts (grain class 8-20 mm). he actual density of the gas phase may be several times higher due to fine dust, which creates a fluidized state in combination with gas. Transport of ejected material in a mixture of gas and dust is much more efficient than transport in a stream of pure gas. However, adopting a lower density value – pure gas – made it possible to determine the minimum transport velocity, using formula (8):

$$v_t = 28{,}6\frac{m}{s} - \sqrt{2 \cdot 9{,}81\frac{m}{s^2} \cdot 0{,}75 \cdot 0{,}014\,m \cdot \frac{2800\frac{kg}{m^3}}{1{,}2\frac{kg}{m^3}}} = 6{,}7\frac{m}{s} \qquad (9)$$

By recording the course of the experiment, it was possible to verify the velocity of individual grains in the gas stream. Several frames that best depict the moving grain have been selected from the video of the experiment. The velocity of the grain was determined based on time elapsed and distance travelled by the grain. Fig. 13 shows three grains moving along the tunnel. The red circle indicates the position of the grain at a given second.
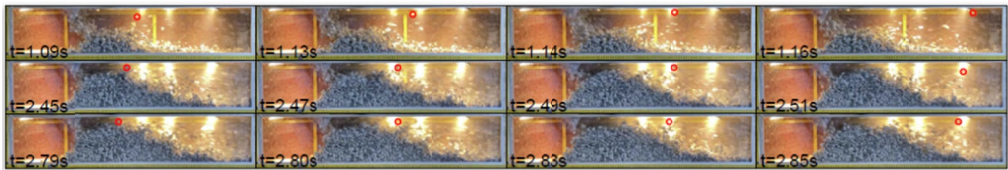

Fig. 13. Recording of the path and time travelled by a grain moving in a gas stream

Table 7 shows the beginning and end of the recorded path of the grain and its determined velocity. The velocity of sample grains determined in the experiment is comparable to the theoretically determined velocity, which was approximately 6.7 m/s.

Based on the results obtained from the theoretical considerations and in the experiments, we can conclude that the proposed interpretation of the force exerted on an individual grain can be used when determining the velocity of transport of ejected material, and therefore when estimating the work done in moving the ejected material.

Experimentally determined velocity of a single grain

No.	Initial position of the grain [cm]	Final position of the grain [cm]	Distance travelled [cm]	Time [s]	Velocity [m/s]
1	35.0	70.5	35.5	0.07	5.1
2	31.5	66.5	35.0	0.06	5.8
3	28.0	64.5	36.5	0.06	6.1

4. Summary

The theoretical considerations and experimental tests allow us to formulate several key conclusions. The analysis of a significant stage of rock and gas outbursts, namely the transport of ejected material, must account for and estimate the main forces exerted on individual grains. These forces primarily include: gravity, reactions with adjoining grains, the force of the gas stream flowing around the grain from the top, and the force exerted by the gas on the front surface of the grain.

This paper describes the effect of the gas stream on the front surface of the grain. From a physical point of view, the force exerted in this case depends on the front surface area of the grain and on the flow rate and density of the gas stream. To confirm the viability of our assumptions, we performed tests that allowed us to verify whether our theory was consistent with experimental data. The test results proved to be consistent with the theoretical analyses.

Furthermore, we performed a theoretical analysis of the velocity of a grain in a gas stream, according to which the velocity of a grain from the 8-20 mm grain size class in a gas stream with a flow rate of approximately 29 m/s was slightly below 7 m/s. These theoretical analyses were also verified by means of an experiment which enabled us to observe the motion of a grain in a gas stream. Based on a recording of the path travelled by the grain during the experiment and its duration, we were able to determine the actual velocity of individual grains. A comparison of theoretical results with the results of the experiment also confirmed the viability of our method of estimating the velocity of a grain.

In the long term, the consistency of the theoretical analyses and experimental data may serve as a model for determining the work needed to transport ejected material, taking into account the calculated grain distribution.

References

[1]   R.D. Lama, J. Bodziony, Management of outburst in underground coal mines. International Journal of Coal Geology **35** (1-4), 83-115 (1998).

[2]   D.J. Black, Review of coal and gas outburst in Australian underground coal mines. International Journal of Mining Science and Technology **29** (6), 815-824 (2019).

[3]   E.Y. Wang, P. Chen, Z.T. Liu, Y.J. Liu, Z.H. Li, X.L. Li, Fine detection technology of gas outburst area based on direct current method in Zhuxianzhuang Coal Mine, China. Safety Science **115**, 12-18 (2019). DOI: https://doi.org/10.1016/j.ssci.2019.01.018

[4]   Ch. Zhang, E. Wang, J. Xu, S. Peng, A new method for coal and gas outburst prediction and prevention based on the fragmentation of ejected coal. Fuel **287**, (2021). DOI: https://doi.org/10.1016/j.fuel.2020.119493

[5]   Ch. Fan, S. Li, M. Luo, W. Du, Z. Yang, Coal and gas outburst dynamic system. International Journal of Mining Science and Technology **27** (1), 49-55 (2017). DOI: https://doi.org/10.1016/j.ijmst.2016.11.003

[6]   F. An, Y. Yuan, X. Chen, Z. Li, L. Li, Expansion energy of coal gas for the initiation of coal and gas outbursts. Fuel **235**, 551-557 (2019). DOI: https://doi.org/10.1016/j.fuel.2018.07.132

[7]   N. Skoczylas, A. Pajdak, K. Kozieł, L.T.P. Braga, Methane Emission during Gas and Rock Outburst on the Basis of the Unipore Model. Energies **12** (10), (2019). DOI: https://doi.org/10.3390/en12101999

[8]   K. Jin, Y. Cheng, T. Ren, W. Zhao, Q. Tu, J. Dong, Z. Wang, B. Hu, Experimental investigation on the formation and transport mechanism of outburst coal-gas flow: Implications for the role of gas desorption in the development stage of outburst. International Journal of Coal Geology **194**, 45-58 (2018).

[9]   J. Cao, H. Sun, B. Wang, L. Dai, B. Zhao, G. Wen, X. Zhao, A novel large-scale three-dimensional apparatus to study mechanisms of coal and gas outburst. International Journal of Rock Mechanics and Mining Sciences **118**, 52-62 (2019).

[10] M. Yankun, H. Xueqiu, L. Zhaohua, A unified model with solid-fluid transition for coal and gas outburst and FEMLIP modelling. Tunnelling and Underground Space Technology **99,** (2020).

[11] T. Majcherczyk, A. Jakubów, Zagrożenia gazodynamiczne w kopalniach Jastrzębskiej Spółki Węglowej SA. Górnictwo i Geoinżynieria **31** (3/1), (2007).

[12] J. Topolnicki, M. Wierzbicki, Transport sedymentacyjny mas powyrzutowych. Prace Instytutu Mechaniki Górotworu PAN **18** (3), 67-73 (2016).

[13] K. Kozieł, N. Skoczylas, K. Soroko, S. Gola, Gas and Dolomite Outbursts in Ore Mines-Analysis of the Phenomenon and the Energy Balance. Energies **13** (11), (2020). DOI: https://doi.org/10.3390/en13112999

[14] K. Kozieł, J. Topolnicki, N. Skoczylas, The Intensity of Heat Exchange between Rock and Flowing Gas in Terms of Gas-Geodynamic Phenomena. Entropy **23** (5), (2021). DOI: https://doi.org/10.3390/e23050556

[15] M. Kudasik, N. Skoczylas, Balancing the amount and composition of gas contained in the pore space of cupriferous rocks. Environmental Earth Sciences **77** (4), (2018). DOI: https://doi.org/10.1007/s12665-018-7331-8

[16] F.H. Hedlund, Past explosive outbursts of entrapped carbon dioxide in salt mines provide a new perspective on the hazards of carbon dioxide. The 4th International Conference on Risk Analysis and Crisis Response (RACR2013), Istanbul, Turkey 2013.

[17] F.H. Hedlund, The extreme carbon dioxide outburst at the Menzengraben potash mine 7 July 1953. Safety Science **50**, 537-553 (2012).

[18] J. Warren-Monday, Gases in Evaporites: Part 1 – Rockbursts and gassy outbursts. Salty Matters, 2016.

[19] B.V. Laptev, R.P. Potekhin, Burst Triggering by Zonal Disintegration of Evaporites Soviet Mining Science **24**, 238-241 (1989).

[20] R. Baltaretu, R. Gaube, A Sudden Outburst of Gas and Rock in Particular Conditions. International Congress on Problems of Sudden Outbursts of Gas and Rock. Leipzig, German Democratic Republic, 1966.

[21] http://www.wug.gov.pl/download/209, Wyższy Urząd Górniczy: Zagrożenia wyrzutami skał i gazów, 2005.

[2]   S.D. Butt, P.K. Frempong, C. Mukherjee, J. Upshamm, Characterization of the permeability and acoustic properties of an outburst-prone sandstone. Journal of Applied Geophysics **58**, 1-12 (2006).

[23] X.Z. Li, A. Hua A, Prediction and prevention of sandstone-gas outbursts in coal mines. International Journal of Rock Mechanics & Mining Sciences **43**, 2-18 (2006).

[24] H. Gil, A. Świdziński, Wyrzuty gazów i skał. Politechnika Śląska. Skrypty Uczelniane, Nr 1366, Wyd. II Gliwice, 1988.

[25] M. Kudasik, N. Skoczylas, Analyzer for measuring gas contained in the pore space in rocks. Measurement Science and Technology **28** (10), (2017).

[26] M. Kudasik, A. Pajdak, N. Skoczylas, The validation process of the method of balancing gas contained in the pore space of rocks via rock comminution. Archives of Mining Sciences **63** (4), 989-1005 (2018).

[27] A. Pajdak, K. Godyń, M. Kudasik, T. Murzyn, The use of selected research methods to describe the pore space of dolomite from copper ore mine, Poland. Environmental Earth Sciences **76**, (2017).

[28] A. Pajdak, M. Kudasik, Structural and textural characteristics of selected copper-bearing rocks as one of the elements aiding in the assessment of gasogeodynamic hazard. Studia Geotechnica et Mechanica **39** (2), 51-59 (2017).

[29] H.R. Parzentny, L. Róg, Dependences between certain petrographic, geochemical and technological indicators of coal quality in the limnic series of the upper silesian coal basin (uscb), Poland. Archives of Mining Sciences **65** (3), 665-684 (2020). DOI: https://doi.org/10.24425/ams.2020.134140

[30] A. Walentek, K. Wierzbiński, Influence of Rock Geomechanical Parameters on Increased Longwall Absolute Methane Emission Rate Forecasting Accuracy. Archives of Mining Sciences **65** (3), 641-664 (2020). DOI: https://doi.org/10.24425/ams.2020.134139

[31] K. Oleszko, M. Młynarczuk, L. Sitek, L. Staš, Application of image processing and different types of imaging devices for three-dimensional imaging of coal grains. Engineering Geology **196**, 286-292 (2015).

[32] X. Gui, H. Xue, R. Gao, X. Zhan, F. Zhao, Study on Structural Performance of Horizontal Axis Wind Turbine with Air Duct for Coal Mine. Energies **15**, (2022). DOI: https://doi.org/10.3390/en15010225

[33] P. Jamróz, Rola świadectw wzorcowania przyrządu pomiarowego w kopalnianych pomiarach. Nowoczesne metody zwalczania zagrożeń aerologicznych w podziemnych wyrobiskach górniczych, GIG, Katowice 2015.

[34] P. Jamróz, Interaction between the Standard and the Measurement Instrument during the Flow Velocity Sensor Calibration Process. Processes **9**, (2021). DOI: https://doi.org/10.3390/pr9101792

[35] P. Wiklak, M. Kulak, M. Lipian, D. Obidowski, Experimental Investigation of the Cooperation of Wind Turbines. Energies **15**, (2022). DOI: https://doi.org/10.3390/en15113906

[36] F. Castellani, A. Eltayesh, F. Natili, T. Tocci, M. Becchetti, L. Capponi, D. Astolfi, G. Rossi, Wind Flow Characterisation over a PV Module through URANS Simulations and Wind Tunnel Optical Flow Methods. Energies **14**, (2021). DOI: https://doi.org/10.3390/en14206546

[37] T. Uchida, K. Sugitani, Numerical and Experimental Study of Topographic Speed-Up Effects in Complex Terrain. Energies **13**, (2020). DOI: https://doi.org/10.3390/en13153896